

# MIND-V: Hierarchical World Model for Long-Horizon Robotic Manipulation with RL-based Physical Alignment

Ruicheng Zhang<sup>1</sup>, Mingyang Zhang<sup>1,5</sup>, Jun Zhou<sup>1</sup>, Zhangrui Guo<sup>3</sup>, Zunnan Xu<sup>1,2\*</sup>, Xiaofan Liu<sup>3</sup>, Zhizhou Zhong<sup>4</sup>, Puxin Yan<sup>4</sup>, Haocheng Luo<sup>1,6†</sup>, and Xiu Li<sup>1†</sup>

<sup>1</sup>Tsinghua University    <sup>2</sup>X Square Robot    <sup>3</sup>Sun Yat-sen University  
<sup>4</sup>HKUST    <sup>5</sup>China University of Geosciences    <sup>6</sup>Central South University

**Abstract.** Scalable embodied intelligence is constrained by the scarcity of diverse, long-horizon robotic manipulation data. Existing video world models in this domain are limited to synthesizing short clips of simple actions and often rely on manually defined trajectories. To this end, we introduce MIND-V, a cognitive hierarchical world model designed to synthesize physically plausible and logically coherent videos of long-horizon robotic manipulation. Inspired by cognitive science, MIND-V bridges high-level reasoning with pixel-level synthesis through three core components: a Semantic Reasoning Hub (SRH) that leverages a pre-trained vision-language model for task planning; a Behavioral Semantic Bridge (BSB) that translates abstract instructions into domain-invariant representations; and a Motor Video Generator (MVG) for conditional video rendering. MIND-V employs Staged Visual Future Rollouts, a test-time optimization strategy to enhance long-horizon robustness. To enforce adherence to physical laws, we introduce a GRPO reinforcement learning post-training phase guided by a novel Physical Foresight Coherence (PFC) reward. PFC leverages the V-JEPA2 world model as a “physics referee” to penalize implausible dynamics in the latent feature space. Experiments confirm MIND-V’s SOTA performance in long-horizon simulation and its significant value for policy learning, introducing a scalable and fully autonomous framework for embodied data synthesis.

**Keywords:** World Model · Video Generation · RL · Embodied AI

## 1 Introduction

Scalable robot learning within Embodied AI [5, 13, 41] is critically bottlenecked by the scarcity of high-quality, diverse, and long-horizon robotic manipulation data [10]. Video world models [1, 7, 54] (VWM) that can simulate physical interactions and predict future outcomes offer a promising solution by potentially synthesizing an infinite stream of robotic operation videos [10, 11, 53].

---

\*Project Lead.

†Corresponding authors.

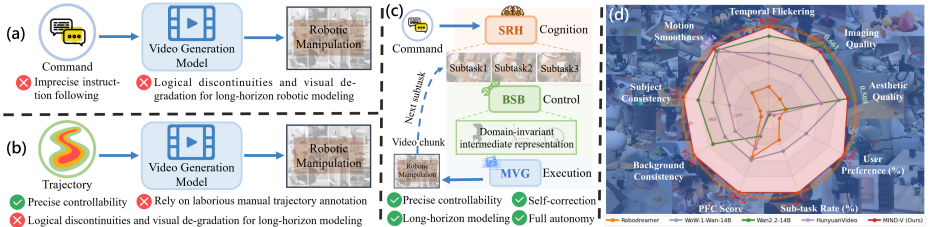


**Fig. 1: Architectural and performance comparison** of MIND-V (c) against the video foundation model (a) and trajectory-controlled generative model (b) paradigms for long-horizon robotic manipulation modeling.

However, constructing a VWM capable of generating high-quality, long-horizon robotic manipulation sequences that faithfully adhere to commands presents three formidable challenges: **(1) Long-Horizon Coherence Challenge:** This demands maintaining causal consistency and logical flow across a sequence of interconnected subtasks, where a single error can compromise the entire operation [14, 39]. **(2) Semantic-to-Pixel Generation Challenge:** This involves accurately translating abstract semantic commands or actions into concrete spatiotemporal interactions in pixel space, which places immense demands on the VWM’s semantic understanding and instruction-following fidelity [22]. **(3) Physical Plausibility Challenge:** The simulated world must ensure strict physical plausibility, requiring adherence to fundamental physical laws governing collision dynamics, object permanence, and interaction forces [25]. Existing methods fail to provide a comprehensive solution to these challenges. On one hand, directly fine-tuning video foundation models [7, 19, 32, 37] for long-horizon robotic modeling often suffer from imprecise instruction following and visual degradation, as they struggle to bridge the vast gap from abstract semantic commands to concrete pixel-level execution (Fig. 1(a)). On the other hand, while trajectory-controlled generative models [10, 34, 35, 54] offer enhanced controllability, they sacrifice the autonomy and scalability essential for large-scale automated data generation, which function more as renderers than as intelligent world simulators (Fig. 1(b)).

To this end, we draw inspiration from the hierarchical theory of human motor control in cognitive science [12]. The human brain executes complex tasks through a hierarchically collaborative process: High-level cognitive centers, such as the cerebral cortex, handle intent understanding and abstract planning, while low-level motor systems, like the cerebellum, translate these plans into precise muscle control. Specialized neural pathways bridge these layers, enabling the efficient translation of abstract intent into concrete physical action [26].

Embracing this paradigm, we introduce **MIND-V**, a cognitive hierarchical world model designed to simulate physically plausible and logically coherent long-horizon robotic manipulations. Emulating the human brain’s “cognition-to-execution pipeline”, MIND-V is built upon three core components (Fig. 1(c)): (1) a **Semantic Reasoning Hub (SRH)** that performs high-level task planning based on a pre-trained Vision-Language Model (VLM); (2) a **Behavioral Semantic Bridge (BSB)** that acts as a domain-invariant link by translat-

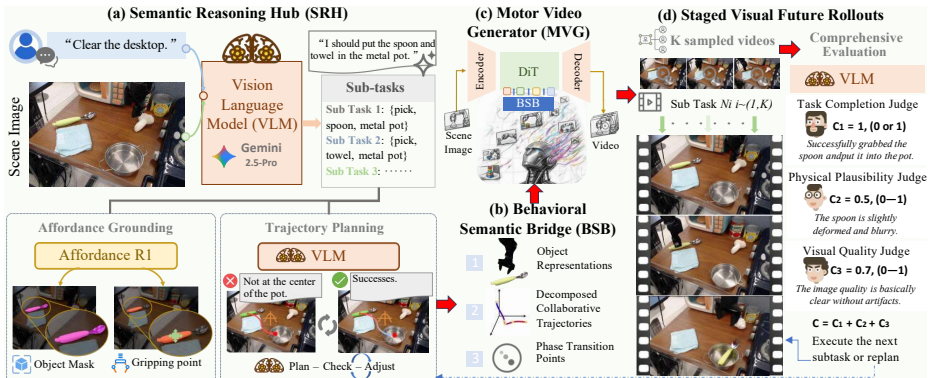


**Fig. 2: Overview of MIND-V: a cognitive hierarchical video world model for long-horizon robotic manipulation.** Beginning in the cognitive core, the Semantic Reasoning Hub (SRH) decomposes a high-level instruction into atomic subtasks and plans detailed trajectories for each. These plans are then encapsulated into the Behavioral Semantic Bridge (BSB), a structured, domain-invariant intermediate representation that serves as a precise blueprint for the Motor Video Generator (MVG). The MVG, a conditional diffusion model, renders photorealistic videos that strictly adhere to the kinematic constraints defined in the BSB. At inference time, Staged Visual Future Rollouts provide a “propose-verify-refine” loop for self-correction, ensuring local optimality at each stage to mitigate error accumulation.

ing abstract plans into structured, executable representations; and (3) a **Motor Video Generator (MVG)** that synthesizes physically realistic manipulation videos conditioned on the BSB. By first generating the BSB through the task reasoning of the SRH and then translating these symbolic representations into embodied action videos with the MVG, MIND-V effectively bridges high-level reasoning with pixel-level synthesis through hierarchical collaboration.

To further align VWM with physical plausibility, we design a novel Group Relative Policy Optimization (GRPO) [20] post-training [43] guided by a Physical Foresight Coherence (PFC) Reward. The PFC reward leverages a pre-trained world model as a “physics referee” to quantify the dynamic coherence of generated videos in latent feature space, thereby aligning the model with physical laws. Furthermore, to mitigate error accumulation in long-horizon tasks, we introduce the Staged Visual Future Rollouts at reference time. Based on the hierarchical architecture, this test-time optimization strategy decomposes the global planning problem into a sequence of locally optimal decisions. At each subtask transition, MIND-V performs a “propose-verify-refine” loop, where it simulates multiple future trajectories and selects the most coherent one to proceed. This staged approach effectively prevents the propagation of early-stage errors and semantic drift, significantly enhancing the fidelity and success rate of the synthesized video.

Our main contributions are as follows:

- To the best of our knowledge, MIND-V is the first hierarchical video world model for long-horizon robotic manipulation tasks. MIND-V effectively bridges

the gap between high-level task planning and low-level pixel synthesis through a three-tier architecture of brain (SRH), symbolic bridge (BSB), and video generator (MVG).

- We present the Staged Visual Future Rollouts, a test-time optimization strategy for VWM that decomposes a global long-horizon generation into a series of locally optimal decisions. By performing a “propose-verify-refine” process at each subtask, this method mitigates error accumulation and enhances generation robustness.
- We propose a GRPO post-training guided by a novel Physical Foresight Coherence (PFC) reward, which leverages a pre-trained world model to score the physical plausibility of generated dynamics in latent feature space, thereby steering the generator towards physically realistic outputs.
- Extensive experiments demonstrate MIND-V’s state-of-the-art performance in long-horizon robotic manipulation video synthesis and highlight its significant downstream application value, thereby establishing a scalable and controllable paradigm for robotic world modeling.

## 2 Related Work

### 2.1 Video World Models for Embodied Intelligence

The advancement of scalable embodied intelligence is critically dependent on large-scale data. However, collecting real-world robotic data is a time-consuming and labor-intensive process. Video World Models (VWM) [19, 30, 32, 37, 49] are capable of predicting future outcomes from current states, emerging as an efficient alternative for synthesizing photorealistic data for policy learning. Models like UniPi [9] and AVDC [18] frame robotic planning as a text-to-video generation problem. WoW [7], Dreamdojo [11] and Robodreamer [53] learn latent physical dynamics from extensive video interaction data to achieve compositional generalization. While these methods demonstrate strong semantic understanding, they lack fine-grained control over the precise execution of manipulation tasks [22]. This gap may lead to logical failures and physical inconsistencies, particularly in long-horizon scenarios. Another category, such as IRASim [54], Cosmos [1] and RoboMaster [10], employs explicit trajectory guidance for more precise control and action modeling. However, these approaches necessitate complex manual annotations, including detailed motion paths and object masks, which severely limits their scalability and autonomy. In contrast, MIND-V’s hierarchical architecture autonomously decomposes high-level commands into executable instructions for the generator, enabling the generation of long-horizon high-fidelity manipulation videos without requiring extra manual guidance.

### 2.2 Controllable Video Generation

Recent advancements in diffusion generation [44, 45] have spurred demand for controllable methods that can accurately translate human intent into visual

content [22]. To this end, research has investigated a spectrum of conditioning modalities to guide the video generation process, ranging from high-level semantic signals (text [32] and audio [51]) to low-level structural inputs (masks [35, 52], trajectories [34, 46], sketches [15, 23], bounding boxes [21], and pose estimations [36, 47]). However, these methods present a fundamental trade-off between semantic abstraction and granular control. High-level semantic conditions like text can provide intuitive guidance but often falls short when dealing with complex multi-stage tasks. This abstraction can lead to semantic drift and diminished fidelity in long-horizon videos, as models struggle to map abstract language onto a consistent sequence of physical interactions [22]. On the other hand, low-level signals such as trajectories, masks, or sketches as conditions can offer more precise spatial and temporal control but imposes a heavy annotation burden, requiring users to specify detailed geometric constraints manually [22]. Our research addresses this dilemma by introducing a hierarchical VWM framework that connects high-level reasoning with pixel-level synthesis. The Semantic Reasoning Hub (SRH) is responsible for interpreting abstract user intentions, while the Behavioral Semantic Bridge (BSB) automatically converts them into structured, multi-dimensional representations for use by the generator. This approach achieves high semantic fidelity and precise control in long-horizon world modeling, obviating the need for auxiliary manual annotations.

## 3 Method

### 3.1 Framework

As illustrated in Fig. 2, MIND-V implements a top-down pipeline from high-level cognition to concrete visual representation. First, the *Semantic Reasoning Hub (SRH)* decomposes a long-horizon task into atomic subtasks based on initial observations and user instructions. For each subtask, the SRH then employs vision modules for affordance localization and trajectory planning to construct a structured, domain-invariant intermediate representation, termed the *Behavioral Semantic Bridge (BSB)*. This representation guides the *Motor Video Generator (MVG)* in synthesizing a photorealistic video sequence. A closed-loop feedback mechanism via *Staged Visual Future Rollouts* returns the generated results to the SRH for evaluation and potential re-planning. A detailed description of each component follows.

**Semantic Reasoning Hub (SRH)** As the cognitive core of our VWM, the SRH translates abstract semantics into actionable geometric signals. It accomplishes this by synergizing two key components: a powerful pre-trained Vision-Language Model (VLM), such as Gemini-2.5-Pro [8], provides long-horizon planning and semantic reasoning, while an affordance-based visual localizer, like Affordance-R1 [33], grounds these plans with physical common sense. This synergy transforms the SRH into a robust, physics-aware decision-making engine.

Given an initial scene observation  $I_0$  and a long-horizon task instruction  $L$  (e.g., “clean the desktop”), the VLM first performs a comprehensive semantic analysis of the scene and then decomposes  $L$  into an ordered sequence of atomic

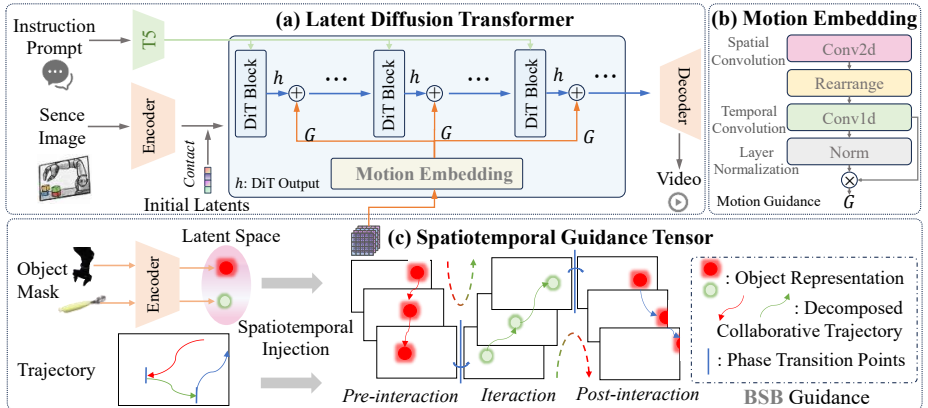


**Fig. 3: Architecture of the Motor Video Generator (MVG).** Serving as the simulation engine, the MVG translates abstract intents (BSB) into concrete visual futures. The process initiates with encoding the BSB’s semantic representation into the (c) Spatiotemporal Guidance Tensor, which embeds the visual features of the active agent along its planned trajectory. This guidance is then processed by the (b) Motion Embedding module to produce refined motion signals ( $G$ ). These signal are finally injected into the (a) Latent Diffusion Transformer, conditioning the denoising process to ensure the synthesized video strictly adheres to the intended physical dynamics.

subtasks. Each subtask is defined by a tuple  $\text{SubTask}_i = \{\text{ActionType}_i, \text{Object}_i, \text{Destination}_i\}$ , which specifies the action primitive, the object of manipulation, and its target location, respectively. This structured decomposition provides a symbolic foundation for precise downstream control generation.

For each subtask, the SRH leverages the affordance localizer’s vision-action alignment capabilities to precisely identify the object’s segmentation mask ( $M_{\text{obj}}$ ) and predict its functional interaction points ( $P_{\text{obj}}$ , e.g., the handle of a cup). Based on this affordance data, the VLM plans a physically plausible trajectory. The trajectory is generated using a smooth curve function and discretized into a sequence of points corresponding to the video frames.

**Behavioral Semantic Bridge (BSB)** The BSB serves as the crucial bridge connecting high-level planning with pixel-level video synthesis. It is a structured domain-invariant intermediate representation that translates symbolic outputs from the SRH into an actionable format for the MVG. The BSB is composed of three key elements:

- **Object Representation:** A set of segmentation masks, including the manipulated object ( $M_{\text{obj}}$ ) and a generic robot arm mask ( $M_{\text{rob}}$ ). A VAE encoder compresses these masks into latent features, which are then injected at specific spatiotemporal locations during video generation to maintain consistent object identity.
- **Decomposed Collaborative Trajectory:** For each subtask, the trajectory is decomposed into three distinct phases: pre-interaction ( $T_{\text{pre}}$ , arm approaches the object), interaction ( $T_{\text{interact}}$ , object is manipulated), and post-interaction ( $T_{\text{post}}$ , arm retracts). This decomposition clearly defines the primary active agent and its objective for each stage [10].

- **Phase Transition Points:** A triplet of frame indices  $(F_{\text{pre}}, F_{\text{interact}}, F_{\text{post}})$  that allocates a specific duration to each of the three phases. This temporal allocation ensures natural motion dynamics and properly emphasizes the core physical interaction.

By decoupling task logic from visual appearance, this design endows the BSB with domain invariance, significantly enhancing the our VWM’s ability to generalize to novel environments and tasks.

**Motor Video Generator (MVG)** As depicted in Fig. 3, the MVG functions as a learnable physics engine. Built upon a Diffusion Transformer (DiT) backbone [27], it is trained to synthesize high-fidelity video sequences that strictly adhere to the kinematic constraints defined by the BSB. To enforce this control, the MVG first encodes the BSB’s object representation into a spatiotemporal guidance tensor of size  $(T \times C \times H \times W)$ . This tensor dynamically embeds the visual features of the active agent (arm or manipulated object) onto its planned path across the time dimension. A motion embedding module integrates this guidance into the DiT backbone during denoising process. The module employs spatiotemporal convolutions to encode the guidance tensor into a feature representation  $G$ . Within each DiT block, this representation is fused with the video’s intermediate hidden state  $h$  via additive fusion:

$$h_{\text{new}} = h + \text{norm}(G) \cdot G, \quad (1)$$

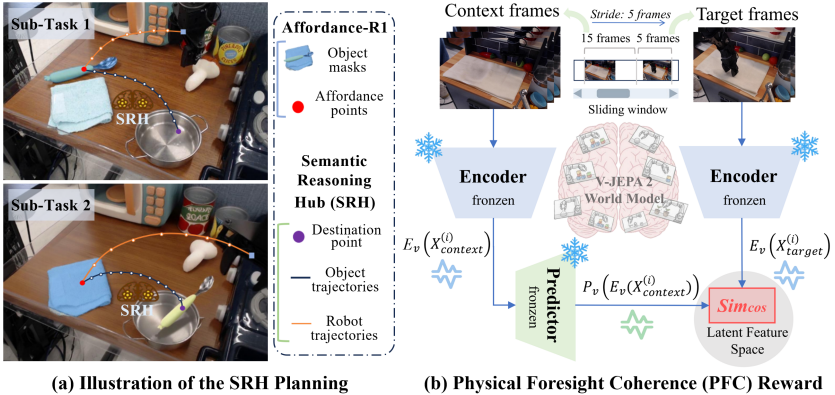
where  $\text{norm}(\cdot)$  denotes Group Normalization to stabilize training. This continuous injection of kinematic constraints compels the model to adhere to the specified trajectory throughout the denoising process, yielding a final video that is both spatiotemporally precise and visually coherent.

### 3.2 Test-Time Optimization via Staged Visual Future Rollouts

Simulating long-horizon futures is plagued by error accumulation, where minor subtask deviations in one subtask cascade into overall task failure [41]. To mitigate this risk, we reframe inference as a search process in the world model’s latent space. We introduce *Staged Visual Future Rollouts*, a novel test-time optimization strategy that mimics “System 2” thinking [40] by deliberating over potential futures at critical decision points.

As illustrated in Fig. 2(d), this mechanism operates as a “Propose-Verify-Refine” loop at each subtask transition. Instead of blindly autoregressing pixels, the SRH first proposes  $K$  semantically plausible candidate plans (i.e., diverse BSBs). The MVG then acts as a parallel simulator, rolling out these plans into short-horizon video clips  $\{V_1, \dots, V_K\}$ . Crucially, the VLM transitions from a planner to a **Critic**, evaluating each rollout based on task success, physical plausibility, and visual quality.

If the highest-scoring video  $V_{\text{top}}$  meets a predefined success threshold, it is selected and the process proceeds. If no candidate is satisfactory, the VLM provides structured textual feedback detailing the failure modes (e.g., “end position



(a) Illustration of the SRH Planning

(b) Physical Foresight Coherence (PFC) Reward

**Fig. 4: (a) Illustration of the SRH Planning. (b) Physical Foresight Coherence (PFC) Reward.** The PFC leverages a frozen V-JEPA2 world model as a “Physics Referee” to predict the latent evolution of future states. The reward quantifies the alignment between the generated video’s dynamics and V-JEPA2’s internal physical laws, computed via cosine similarity in the predictive latent space.

error”, “object not grasped correctly”). This feedback loop instructs the SRH to re-plan and propose a refined set of masks and trajectories in the next iteration. This iterative cycle of propose-verify-refine transforms the VWM from a simple feed-forward predictor into a proactive, self-correcting agent, significantly enhancing the robustness and success rate of long-horizon task simulations.

### 3.3 MVG Training: From SFT to RL Alignment

To establish MVG as a physically grounded simulator, we employ a two-stage training paradigm. First, Supervised Fine-Tuning (SFT) adapts a pre-trained video model to the robotics domain. This is followed by a GRPO Reinforcement Learning (RL) post-training phase that aligns the model’s internal dynamics with fundamental physical laws and aesthetic standards.

**Stage 1: Supervised Fine-Tuning (SFT)** The SFT phase adapts a video foundation model to learn the fundamental mapping from the structured Behavioral Semantic Bridge (BSB) to coherent pixel-level execution. We fine-tune the video foundation model on a real-world robotics dataset (e.g., Bridge v2 [31]) using ground-truth BSB annotations. The optimization minimizes the standard denoising objective conditioned on the BSB:

$$\mathcal{L}_{\text{SFT}}(\theta) = \mathbb{E}_{(x_0, \text{BSB}) \sim \mathcal{D}, \epsilon \sim \mathcal{N}(0, I), t} [\|\epsilon - \epsilon_\theta(x_t, t, \text{BSB})\|^2], \quad (2)$$

where  $x_t$  is the noised video at timestep  $t$ . This stage provides a high-quality initial policy  $\pi_{\text{ref}}$  for the subsequent alignment phase. Notably, the model only needs to be trained on short subtask videos, as the hierarchical framework enables generalization to arbitrary long-horizon tasks.

**Stage 2: Physical Alignment via GRPO Post-Training** While SFT enforces motion adherence, it cannot guarantee physical plausibility or aesthetic quality of the generated videos, objectives that are ill-suited for conventional

loss functions [20]. To bridge this gap, we introduce a post-training alignment stage using Reinforcement Learning (RL). This stage models the denoising process as a Markov Decision Process (MDP) and employs Group Relative Policy Optimization (GRPO) [20] for optimization.

The optimization is guided by a composite reward function  $R(x_0)$  that assesses the overall quality of the generated video  $x_0$  via a weighted combination of a physics-based reward and an aesthetic reward:

$$R(x_0) = w_p \cdot R_{\text{physics}}(x_0) + w_a \cdot R_{\text{aesthetic}}(x_0), \quad (3)$$

with  $w_p = 0.2$  and  $w_a = 1$ . Ablation details are presented in Sec. 4.4.

**Physical Foresight Coherence (PFC) Reward ( $R_{\text{physics}}$ ):** This reward innovatively employs a powerful pre-trained world model, V-JEPA2 [2], as a ‘‘Physics Referee’’. Pre-trained via self-supervision on large-scale real-world data and fine-tuned on robotics datasets, V-JEPA2 acquires an internal model of world dynamics, enabling it to accurately understand the existing state and predict future states within an abstract latent space. For each generated video, a sliding window approach is employed to assess local physical plausibility. The consistency score  $s_i$  for each window is the cosine similarity between V-JEPA2’s latent prediction and the actual future (Fig. 4):

$$PFC : s_i = \text{sim}_{\cos} \left( P_v(E_v(x_{\text{context}}^{(i)})), E_v(x_{\text{target}}^{(i)}) \right), \quad (4)$$

where  $E_v$  and  $P_v$  are V-JEPA2’s visual encoder and predictor, respectively. To concentrate optimization on the most egregious physical violations, we employ a softmax-based weighting scheme to assign higher weights to windows with larger physical errors  $(1 - s_i)$ :

$$R_{\text{physics}}(x_0) = \sum_{i=1}^{N_w} \frac{\exp((1 - s_i)/\tau)}{\sum_{j=1}^{N_w} \exp((1 - s_j)/\tau)} \cdot s_i. \quad (5)$$

Here, the temperature parameter  $\tau$  controls the focus: a lower  $\tau$  value concentrates the reward on the single worst-offending window. By leveraging the world model’s robust understanding and prediction capability of physical evolution, the PFC reward transforms the evaluation from a rigid assessment into a targeted optimization of dynamic causal chains, significantly improving the physical consistency of generated actions [38].

**Aesthetic Reward ( $R_{\text{aesthetic}}$ ):** The aesthetic reward is provided by a VLM, such as Gemini 2.5 [8]. The VLM assesses each video for clarity, artifacts, and realism, assigning a discrete integer score (e.g., 1-5), which yields a stable and discriminative reward signal for optimization.

**GRPO Optimization:** GRPO is an efficient, value-free policy optimization algorithm. At each optimization step, we sample a group of  $G$  videos  $\{x_0^i\}_{i=1}^G$  from the current policy  $\pi_\theta$ . The advantage  $\hat{A}^i$  for each sample is then computed by normalizing its reward relative to the group’s statistics:

$$\hat{A}^i = \frac{R(x_0^i) - \text{mean}(\{R(x_0^j)\}_{j=1}^G)}{\text{std}(\{R(x_0^j)\}_{j=1}^G)}, \quad (6)$$

where  $\text{mean}(\cdot)$  and  $\text{std}(\cdot)$  denote the mean and standard deviation of the rewards within the group. This group-relative normalization provides a stable advantage estimation without requiring a separate critic network. The policy is then updated by maximizing the standard GRPO objective function:

$$\mathcal{J}_{\text{GRPO}}(\theta) = \mathbb{E} \left[ \frac{1}{G} \sum_{i=1}^G \left( \min \left( r_i(\theta) \hat{A}^i, \text{clip}(r_i(\theta), 1 - \epsilon, 1 + \epsilon) \hat{A}^i \right) - \beta D_{\text{KL}}(\pi_\theta \| \pi_{\text{ref}}) \right) \right] \quad (7)$$

where  $r_i(\theta) = \frac{\pi_\theta(x_0^i)}{\pi_{\text{ref}}(x_0^i)}$  is the importance sampling ratio,  $\epsilon$  is a clipping hyperparameter that ensures conservative policy updates, and the KL-divergence term regularizes the policy towards the SFT policy  $\pi_{\text{ref}}$  to mitigate reward hacking and maintain generation quality. This optimization process progressively aligns the MVG towards higher physical fidelity and aesthetic quality while maintaining its adherence to kinematic conditioning.

## 4 Experiments

### 4.1 Experiment Settings

**Architecture and Training** Our Semantic Reasoning Hub (SRH) employs Gemini-2.5 Pro API [8] as its core Vision-Language Model (VLM), complemented by Affordance-R1 [33] as visual localizer. The Motor Video Generator (MVG) is initialized from the pre-trained CogVideoX-5B [37] architecture. Experiments are conducted on the Bridge V2 [31] dataset, following the data processing protocol established in [10]. We adopt a resolution of  $480 \times 640$  pixels and a video length of 37 frames per subtask for both training and inference. The model underwent two training stages: (1) Supervised fine-tuning (SFT) for 30,000 steps with an AdamW optimizer and a learning rate of  $2 \times 10^{-5}$ ; and (2) GRPO post-training for 1,500 iterations at a learning rate of  $5 \times 10^{-5}$ . At inference time, MIND-V can generate a 111-frame long-horizon video (comprising three subtasks) with around 50 GB of VRAM. Theoretically, due to its autoregressive, subtask-based architecture, MIND-V can generate arbitrarily long task-sequence videos with only a linear increase in computational cost. All experiments are conducted on four NVIDIA H200 GPUs. Additional implementation details are provided in the **supplementary material**.

**Evaluation Protocol and Metrics** The evaluation is performed on a test set of 108 samples. This set comprises scenes from the Bridge V2 test set [31] and unseen scenes sourced from the web. Recognizing that different task horizons demand different evaluation criteria, we adopt a bifurcated protocol. For short-horizon tasks, our evaluation focuses exclusively on *visual quality*, where we use V-Bench [50] for evaluation. For long-horizon tasks, we introduce user study and two additional metrics: (1) *physical plausibility*, which is quantified by our Physical Foresight Coherence (PFC) score, as detailed in Section 3.3; and (2) *Task Success Rate*, which measures the average success rate across all subtasks of the entire long-horizon task.

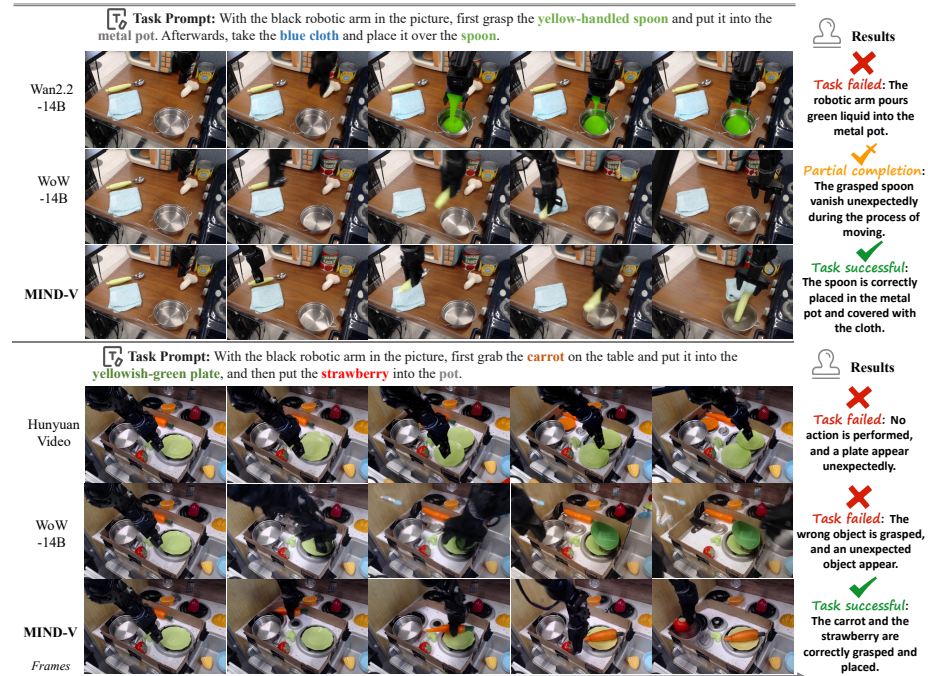


**Fig. 5: Qualitative comparison of long-horizon robotic manipulation video generation.** The baseline models exhibit significant deficiencies, including logical inconsistencies, physical implausibility, and poor semantic grounding. In contrast, MIND-V successfully executes long-horizon instructions with high visual quality and physical fidelity. This validates the efficacy of our hierarchical architecture, which decouples high-level reasoning from pixel-level synthesis to ensure robust long-horizon coherence and spatiotemporal precision.

**Baselines and Comparative Setup** For short-horizon task, we benchmark MIND-V against both autonomous world models (Dreamdojo [11], Robodreamer [53], WoW [7], CogVideoX-5B [37], HunyuanVideo [19]) and trajectory-guided methods (IRASim [54], Cosmos [1], MotionCtrl [34], DragAnything [35], Tora [48]). Among them, video foundation models such as CogVideoX-5B and HunyuanVideo are fine-tuned on our dataset for fair comparison. It is crucial to note that trajectory-based models receive privileged information at inference time, such as manual trajectories, masks, or anchor points, which is unavailable to our trajectory-free approach. This distinction highlights MIND-V’s capability to infer complex dynamics solely from high-level intent. For long-horizon task, which emphasizes complex planning and reasoning without explicit guidance, our comparison is focused on SOTA autonomous world models (Dreamdojo, Robodreamer, WoW, CogVideoX-5B and HunyuanVideo). Each long-horizon task in our benchmark is composed of a sequence of 2 to 4 subtasks, designed to probe the limits of long-horizon planning and generation.

**Table 1:** Visual quality evaluation on short-horizon and long-horizon tasks. Higher is better; best and second-best results are highlighted.

Method	Aesthetic Quality $\uparrow$	Imaging Quality $\uparrow$	Temporal Flicker $\uparrow$	Motion Smoothness $\uparrow$	Subject Consistency $\uparrow$	Bg. Consistency $\uparrow$
<b>Short-horizon Tasks</b>						
MotionCtrl [34]	0.491	0.665	0.977	0.972	0.915	0.942
IRASim [54]	0.504	0.676	0.979	0.986	0.929	0.957
Cosmos [1]	0.519	0.680	0.980	0.988	0.932	0.958
DragAnything [35]	0.500	0.679	0.980	0.983	0.935	0.957
Tora [48]	0.509	0.670	0.981	0.984	0.922	0.961
RoboMaster [10]	0.502	<b>0.688</b>	0.982	0.981	0.937	0.950
Robodreamer [53]	0.511	0.680	0.977	0.976	0.930	0.945
WoW-1-DiT-7B [7]	0.522	0.682	0.982	0.985	0.933	0.960
<b>MIND-V (Ours)</b>	<b>0.526</b>	0.684	<b>0.986</b>	<b>0.991</b>	<b>0.940</b>	<b>0.963</b>
<b>Long-horizon Tasks</b>						
Robodreamer [53]	0.464	0.628	0.910	0.918	0.839	0.885
WoW-1-DiT-7B [7]	0.476	0.635	0.922	0.929	0.851	0.894
WoW-1-Wan-14B [7]	0.498	0.652	0.935	0.950	0.874	0.906
Dreamdojo [11]	0.504	<b>0.660</b>	0.944	0.948	0.883	0.909
HunyuanVideo [19]	0.487	0.643	0.928	0.952	0.862	0.900
CogVideoX-5B [37]	0.484	0.640	0.926	0.947	0.860	0.895
<b>MIND-V (Ours)</b>	<b>0.512</b>	0.658	<b>0.955</b>	<b>0.953</b>	<b>0.896</b>	<b>0.924</b>

## 4.2 Qualitative and Quantitative Comparison

As demonstrated in Fig. 5 and Tables 1–2, MIND-V consistently outperforms state-of-the-art baselines, establishing a new standard for both short- and long-horizon robotic simulation tasks. In long-horizon tasks, MIND-V surpasses the second-best method by 9.0%, 76.7%, and 172.2% on PFC Score, Task Success Rate, and User Preference, respectively. Baseline models consistently struggle with task execution and long-horizon coherence (Table 2). They exhibit critical deficiencies (Fig. 5(a)), including logical failures (e.g., hallucinating unprompted actions), physical implausibility (e.g., spontaneous object disappearance), and inaccurate semantic grounding (e.g., incorrect object manipulation).

In contrast, MIND-V successfully executes these long-horizon tasks, demonstrating robust adherence to both instructions and physical principles. This superior performance is attributed to our cognitive hierarchical design: The *Semantic Reasoning Hub (SRH)* and *Behavioral Semantic Bridge (BSB)* collaborate to decompose user instructions into an explicit, executable plan, which mitigates the risk of semantic drift common in end-to-end models.

Subsequently, the *Motor Video Generator (MVG)*, aligned via with our Physical Foresight Coherence (PFC) reward, synthesizes simulation videos that strictly adhere to physical laws and command requirements. Furthermore, the *Staged*

**Table 2:** Comprehensive evaluation of long-horizon tasks (PFC Score, Task Success Rate, and User Preferences). Higher is better; best results are bolded.

Method	PFC Score $\uparrow$	Task Success Rate	User Pref. (%) $\uparrow$
Dreamdojo [11]	0.424	0.333	18
Robodreamer [53]	0.418	0.275	7
WoW-1-DiT-7B [7]	0.423	0.322	11
WoW-1-Wan-14B [7]	0.420	0.347	14
CogVideoX-5B [37]	0.406	0.081	0
HunyuanVideo [19]	0.411	0.098	1
<b>MIND-V (Ours)</b>	<b>0.462</b>	<b>0.613</b>	<b>49</b>

*Visual Future Rollouts* effectively prevents the error accumulation that plagues baseline methods, enabling the generation of coherent and physically plausible manipulation sequences.

### 4.3 World Model for Policy Learning

To validate the utility of MIND-V as a training ground for embodied agents, we conduct a “Generation-to-Policy” experiment in the MimicGen simulation benchmark [24] (Fig. 6). We select three fine-grained manipulation tasks (Coffee, Stack-Three, Square) with a limited budget of 128 demonstration trajectories per task.

**Setup** We first fine-tune a VLA (OpenVLA-OFT [16]) via imitation learning (IL) with 300 expert trajectories on target manipulation tasks as base policy. For comparison, the IL training strategy continues training this OpenVLA-OFT model using end-effector pose supervision ( $\mathcal{L}_{\text{pose}}$ ) until convergence. In our approach, in addition to the standard pose loss, we leverage MIND-V to generate successful visual rollouts ( $o$ ) conditioned on the task instructions, which serve as visual goals to guide the VLA policy. Specifically, the OpenVLA-OFT predicts an action sequence to execute a rollout ( $\hat{o}$ ) in simulation engine, which is supervised by minimizing the visual discrepancy against MIND-V’s prediction:

$$\mathcal{L} = \lambda_{\text{pix}} \|\hat{o} - o\|_1 + \lambda_{\text{perc}} d_{\text{LPIPS}}(\hat{o}, o) + \lambda_{\text{IL}} \mathcal{L}_{\text{pose}}, \quad (8)$$

where  $\|\hat{o} - o\|_1$  and  $d_{\text{LPIPS}}(\hat{o}, o)$  denote the  $L_1$  pixel reconstruction loss and LPIPS perceptual loss [42], respectively.

**Discussion** As detailed in Table 3, incorporating MIND-V significantly raises the performance ceiling of the VLA policy: the mean success rate improves from 27.7% (Base) to **43.5%** with MIND-V guidance, far exceeding the 33.4% of IL continuous learning strategy. This result underscores a fundamental advantage of pixel-space world models: unlike latent-space IL or RL approaches that operate in abstract representations detached from visual reality, MIND-V generates futures in the same pixel space as the VLA’s pre-training data. This alignment allows the VLA to directly leverage its rich visual priors to learn from the world model’s imagined rollouts, effectively bridging the gap between generative world simulation and actionable policy learning [55].

### 4.4 Ablation Study

**Component Contribution Analysis** To evaluate the contribution of each core component, we compare the full MIND-V model against four ablated vari-

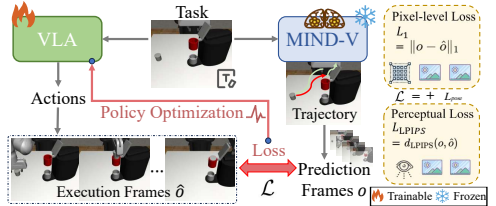


**Fig. 6: Illustration of downstream policy learning with MIND-V.**

**Table 3: Task success rates (%) under different training paradigms in the MimicGen simulation benchmark. Best results are **bolded**.**

Methods	Coffee	StackThree	Square	Mean
Base policy	32.6	30.2	20.2	27.7
IL	37.4	36.7	26.1	33.4
<b>MIND-V + IL</b>	<b>51.7</b>	<b>48.3</b>	<b>30.4</b>	<b>43.5</b>

**Table 4:** Ablation study on long-horizon simulation tasks. Visual quality (Aesthetic and Imaging Quality) and functional correctness (PFC Score and subtask Average Success Rate) are reported. Best results are **bolded**.

Model Variant	Visual Quality		Functional Correctness	
	Aesthetic $\uparrow$	Imaging $\uparrow$	PFC Score $\uparrow$	subtask Avg. $\uparrow$
(a) w/o GRPO	0.491	0.675	0.429	0.582
(b) Re Affordance w/ YOLO+SAM2	0.498	0.680	0.445	0.455
(c) w/o Staged Rollouts	0.482	0.671	0.438	0.327
(d) Re Gemini w/ Qwen3-VL	0.500	0.679	0.452	0.567
<b>MIND-V (Full)</b>	<b>0.504</b>	<b>0.684</b>	<b>0.462</b>	<b>0.613</b>

ants on long-horizon simulation: (a) **w/o GRPO**: trained solely with SFT, without GRPO post-training stage; (b) **Re Affordance w/ YOLO+SAM2**: replacing the affordance localizer [33] in BSB with a YOLO-World [6] + SAM2 [28] pipeline; (c) **w/o Staged Rollouts**: disabling the test-time staged optimization mechanism; (d) **Re Gemini w/ Qwen3-VL**: substituting Gemini 2.5 Pro in SRH with Qwen3-VL [4] to test VLM dependence.

As shown in Table 4, the full model outperforms all ablated variants, confirming the necessity of each component. Removing GRPO results in a clear decline in PFC Score, underscoring the effectiveness of our RL-based alignment in improving physical plausibility. Replacing the affordance module with an alternative pipeline causes a substantial drop in subtask success rates, highlighting its critical role in enabling functional grounding for manipulation in BSB. Disabling staged rollouts leads to pronounced performance degradation, demonstrating proposing and verifying futures (“System 2 thinking” [40]) is essential for mitigating error accumulation over extended horizons. Switching the VLM in SRH yields a marginal drop, indicating that a powerful VLM is beneficial for improving performance, but MIND-V does not rely on a specific VLM model.

### Reward Sensitivity Analysis

These parameters  $w_a$  and  $w_p$  in Eq. 3 serve to normalize reward scales to the same order of magnitude. The sensitivity analysis

**Table 5:** Sensitivity analysis of reward weights.

$w_a$	$w_p$	Aesthetic $\uparrow$	Imaging $\uparrow$	PFC Score $\uparrow$	subtask Avg. $\uparrow$
0.5	0.2	0.498	0.651	<b>0.449</b>	0.612
<b>1.0</b>	<b>0.2</b>	<u>0.504</u>	<b>0.658</b>	<u>0.445</u>	<b>0.613</b>
2.0	0.2	<b>0.508</b>	0.657	0.434	0.562

(Table 5) on long-horizon tasks shows robust performance across a reasonable range and the rationality of our parameter selection.

## 5 Conclusion

In this work, we introduce **MIND-V**, a cognitive hierarchical video world model designed to simulate the physical reality of long-horizon robotic manipulation. Drawing inspiration from the human brain’s cognition-to-execution pathway, MIND-V integrates three core modules: the Semantic Reasoning Hub (SRH), the Behavioral Semantic Bridge (BSB), and the Motor Video Generator (MVG). By decoupling high-level semantic reasoning from low-level pixel synthesis, MIND-V successfully addresses the key challenges of long-horizon coherence, semantic grounding, and physical plausibility. The efficacy of our approach is further enhanced by two key innovations: a GRPO post-training phase with a Physical Foresight Coherence (PFC) reward that enforces alignment with physical laws;

and a test-time optimization via staged visual future rollouts that mitigates error accumulation over extended horizons. Comprehensive experiments demonstrate that MIND-V not only achieves SOTA performance in video synthesis but also serves as an effective training ground for embodied AI policies.

## References

1. Agarwal, N., Ali, A., Bala, M., Balaji, Y., Barker, E., Cai, T., Chattopadhyay, P., Chen, Y., Cui, Y., Ding, Y., et al.: Cosmos world foundation model platform for physical ai. arXiv preprint arXiv:2501.03575 (2025)
2. Assran, M., Bardes, A., Fan, D., Garrido, Q., Howes, R., Komeili, M., Muckley, M., Rizvi, A., Roberts, C., Sinha, K., Zhohus, A., Arnaud, S., Gejji, A., Martin, A., Hogan, F.R., Dugas, D., Bojanowski, P., Khalidov, V., Labatut, P., Massa, F., Szafraniec, M., Krishnakumar, K., Li, Y., Ma, X., Chandar, S., Meier, F., LeCun, Y., Rabbat, M., Ballas, N.: V-jepa 2: Self-supervised video models enable understanding, prediction and planning. arXiv preprint arXiv:2506.09985 (2025)
3. Bai, J., Bai, S., Yang, S., Wang, S., Tan, S., Wang, P., Lin, J., Zhou, C., Zhou, J.: Qwen-vl: A versatile vision-language model for understanding, localization, text reading, and beyond. arXiv preprint arXiv:2308.12966 (2023)
4. Bai, S., Cai, Y., Chen, R., Chen, K., Chen, X., Cheng, Z., Deng, L., Ding, W., Gao, C., Ge, C., et al.: Qwen3-vl technical report. arXiv preprint arXiv:2511.21631 (2025)
5. Black, K., Brown, N., Driess, D., Esmail, A., Equi, M., Finn, C., Fusai, N., Groom, L., Hausman, K., Ichter, B., Jakubczak, S., Jones, T., Ke, L., Levine, S., Li-Bell, A., Mothukuri, M., Nair, S., Pertsch, K., Shi, L.X., Tanner, J., Vuong, Q., Walling, A., Wang, H., Zhilinsky, U.:  $\pi_0$ : A vision-language-action flow model for general robot control. arXiv preprint arXiv:2410.24164 (2024)
6. Cheng, T., Song, L., Ge, Y., Liu, W., Wang, X., Shan, Y.: Yolo-world: Real-time open-vocabulary object detection. In: Proceedings of the IEEE/CVF Conference on Computer Vision and Pattern Recognition (CVPR). pp. 1234–1245. IEEE (2024)
7. Chi, X., Jia, P., Fan, C.K., Ju, X., Mi, W., Qin, Z., Zhang, K., Tian, W., Ge, K., Li, H., et al.: Wow: Towards a world omniscient world model through embodied interaction. arXiv preprint arXiv:2509.22642 (2025)
8. Comanici, G., Bieber, E., Schaekermann, M., Pasupat, I., Sachdeva, N., Dhillon, I., Blistein, M., Ram, O., Zhang, D., Rosen, E., Marris, L., Petulla, S.: Gemini 2.5: Pushing the frontier with advanced reasoning, multimodality, long context, and next generation agentic capabilities. arXiv preprint arXiv:2507.06261 (2025)
9. Du, Y., Yang, S., Dai, B., Dai, H., Nachum, O., Tenenbaum, J.B., Schuurmans, D., Abbeel, P.: Learning universal policies via text-guided video generation. In: Advances in Neural Information Processing Systems (NeurIPS). vol. 36, pp. 9156–9172. Curran Associates, Inc. (2023)
10. Fu, X., Wang, X., Liu, X., Bai, J., Xu, R., Wan, P., Zhang, D., Lin, D.: Learning video generation for robotic manipulation with collaborative trajectory control. arXiv preprint arXiv:2506.01943 (2025)
11. Gao, S., Liang, W., Zheng, K., Malik, A., Ye, S., Yu, S., Tseng, W.C., Dong, Y., Mo, K., Lin, C.H., Ma, Q., Nah, S., Magne, L., Xiang, J., Xie, Y., Zheng, R., Niu, D., Tan, Y.L., Zentner, K.R., Kurian, G., Indupuru, S., Jannaty, P., Gu, J., Zhang, J., Malik, J., Abbeel, P., Liu, M.Y., Zhu, Y., Jang, J., Fan, L.J.: Dreamdojo: A generalist robot world model from large-scale human videos. arXiv preprint arXiv:2602.06949 (2026)

12. Grillner, S.: Neurobiological bases of rhythmic motor acts in vertebrates. *Science* **228**(4696), 143–149 (1985)
13. Huang, W., Wang, C., Li, Y., Zhang, R., Fei-Fei, L.: Rekep: Spatio-temporal reasoning of relational keypoint constraints for robotic manipulation. arXiv preprint arXiv:2409.01652 (2024)
14. Ji, Y., Tan, H., Shi, J., Hao, X., Zhang, Y., Zhang, H., Wang, P., Zhao, M., Mu, Y., An, P., et al.: Robobrain: A unified brain model for robotic manipulation from abstract to concrete. In: Proceedings of the IEEE/CVF Conference on Computer Vision and Pattern Recognition (CVPR). pp. 1724–1734. IEEE (2025)
15. Jiang, L., Chen, S., Wu, B., Guan, X., Zhang, J.: Vidsketch: Hand-drawn sketch-driven video generation with diffusion control. arXiv preprint arXiv:2502.01101 (2025)
16. Kim, M.J., Finn, C., Liang, P.: Fine-tuning vision-language-action models: Optimizing speed and success. arXiv preprint arXiv:2502.19645 (2025)
17. Kingma, D.P., Welling, M.: Auto-encoding variational bayes. arXiv preprint arXiv:1312.6114 (2022)
18. Ko, P.C., Mao, J., Du, Y., Sun, S.H., Tenenbaum, J.B.: Learning to act from actionless videos through dense correspondences. arXiv preprint arXiv:2310.08576 (2023)
19. Kong, W., Tian, Q., Zhang, Z., Min, R., Dai, Z., Zhou, J., Xiong, J., Li, X., Wu, B., Zhang, J., et al.: Hunyuanvideo: A systematic framework for large video generative models. arXiv preprint arXiv:2412.03603 (2024)
20. Liu, J., Liu, G., Liang, J., Li, Y., Liu, J., Wang, X., Wan, P., Zhang, D., Ouyang, W.: Flow-grpo: Training flow matching models via online rl. arXiv preprint arXiv:2505.05470 (2025)
21. Liu, Z., Xu, Z., Shu, S., Zhou, J., Zhang, R., Tang, Z., Li, X.: Controllable layer decomposition for reversible multi-layer image generation. arXiv preprint arXiv:2511.16249 (2025)
22. Ma, Y., Feng, K., Hu, Z., Wang, X., Wang, Y., Zheng, M., He, X., Zhu, C., Liu, H., He, Y., et al.: Controllable video generation: A survey. arXiv preprint arXiv:2507.16869 (2025)
23. Ma, Y., Liu, H., Wang, H., Pan, H., He, Y., Yuan, J., Zeng, A., Cai, C., Shum, H.Y., Liu, W., et al.: Follow-your-emoji: Fine-controllable and expressive freestyle portrait animation. In: SIGGRAPH Asia 2024 Conference Papers. pp. 1–12. ACM (2024)
24. Mandlekar, A., Nasiriany, S., Wen, B., Akinola, I., Narang, Y., Fan, L., Zhu, Y., Fox, D.: Mimicgen: A data generation system for scalable robot learning using human demonstrations. In: 7th Annual Conference on Robot Learning (CoRL). PMLR (2023)
25. Meng, S., Luo, Y., Liu, P.: Grounding creativity in physics: a brief survey of physical priors in aigc. In: Proceedings of the Thirty-Fourth International Joint Conference on Artificial Intelligence (IJCAI). IJCAI (2025), article No. 1176
26. Merel, J., Botvinick, M., Wayne, G.: Hierarchical motor control in mammals and machines. *Nature Communications* **10**(1), 5489 (2019)
27. Peebles, W., Xie, S.: Scalable diffusion models with transformers. In: Proceedings of the IEEE/CVF International Conference on Computer Vision (ICCV). pp. 4195–4205. IEEE (2023)
28. Ravi, N., Gabeur, V., Hu, Y.T., Hu, R., Ryali, C., Ma, T., Khedr, H., Rädle, R., Rolland, C., Gustafson, L., Mintun, E., Pan, J., Alwala, K.V., Carion, N., Wu, C.Y., Girshick, R., Dollár, P., Feichtenhofer, C.: Sam 2: Segment anything in images and videos. arXiv preprint arXiv:2408.00714 (2024)

29. Ren, T., Liu, S., Zeng, A., Lin, J., Li, K., Cao, H., Chen, J., Huang, X., Chen, Y., Yan, F., Zeng, Z., Zhang, H., Li, F., Yang, J., Li, H., Jiang, Q., Zhang, L.: Grounded sam: Assembling open-world models for diverse visual tasks. arXiv preprint arXiv:2401.14159 (2024)
30. Team, I., Feng, T., Han, Y., He, J., He, Y., Lin, X., Liu, T., Lu, H., Tang, J., Wang, W., et al.: Inferix: A block-diffusion based next-generation inference engine for world simulation. arXiv preprint arXiv:2511.20714 (2025)
31. Walke, H., Black, K., Lee, A., Kim, M.J., Du, M., Zheng, C., Zhao, T., Hansen-Estruch, P., Vuong, Q., He, A., Myers, V., Fang, K., Finn, C., Levine, S.: Bridge-data v2: A dataset for robot learning at scale. In: Conference on Robot Learning (CoRL). PMLR (2023)
32. Wan, T., Wang, A., Ai, B., Wen, B., Mao, C., Xie, C.W., Chen, D., Yu, F., Zhao, H., Yang, J., Zeng, J., Wang, J., Zhang, J., Zhou, J., Wang, J., Chen, J., Zhu, K., Zhao, K., Yan, K., Huang, L., Feng, M., Zhang, N., Li, P., Wu, P., Chu, R., Feng, R., Zhang, S., Sun, S., Fang, T., Wang, T., Gui, T., Weng, T., Shen, T., Lin, W., Wang, W., Wang, W., Zhou, W., Wang, W., Shen, W., Yu, W., Shi, X., Huang, X., Xu, X., Kou, Y., Lv, Y., Li, Y., Liu, Y., Wang, Y., Zhang, Y., Huang, Y., Li, Y., Wu, Y., Liu, Y., Pan, Y., Zheng, Y., Hong, Y., Shi, Y., Feng, Y., Jiang, Z., Han, Z., Wu, Z.F., Liu, Z.: Wan: Open and advanced large-scale video generative models. arXiv preprint arXiv:2503.20314 (2025)
33. Wang, H., Wang, S., Zhong, Y., Yang, Z., Wang, J., Cui, Z., Yuan, J., Han, Y., Liu, M., Ma, Y.: Affordance-r1: Reinforcement learning for generalizable affordance reasoning in multimodal large language model. arXiv preprint arXiv:2508.06206 (2025)
34. Wang, Z., Yuan, Z., Wang, X., Li, Y., Chen, T., Xia, M., Luo, P., Shan, Y.: Motionctrl: A unified and flexible motion controller for video generation. In: ACM SIGGRAPH 2024 Conference Papers. pp. 1–11. ACM (2024)
35. Wu, W., Li, Z., Gu, Y., Zhao, R., He, Y., Zhang, D.J., Shou, M.Z., Li, Y., Gao, T., Zhang, D.: Draganything: Motion control for anything using entity representation. In: European Conference on Computer Vision (ECCV). pp. 331–348. Springer (2024)
36. Xu, Z., Yu, Z., Zhou, Z., Zhou, J., Jin, X., Hong, F.T., Ji, X., Zhu, J., Cai, C., Tang, S., et al.: Hunyuanportrait: Implicit condition control for enhanced portrait animation. In: Proceedings of the IEEE/CVF Conference on Computer Vision and Pattern Recognition (CVPR). pp. 15909–15919. IEEE (2025)
37. Yang, Z., Teng, J., Zheng, W., Ding, M., Huang, S., Xu, J., Yang, Y., Hong, W., Zhang, X., Feng, G., et al.: Cogvideox: Text-to-video diffusion models with an expert transformer. arXiv preprint arXiv:2408.06072 (2024)
38. Yuan, J., Zhang, X., Friedrich, F., Beltran-Velez, N., Hall, M., Askari-Hemmat, R., Han, X., Ballas, N., Drodzdzal, M., Romero-Soriano, A.: Improving the physics of video generation with vjpa-2 reward signal. arXiv preprint arXiv:2510.21840 (2025)
39. Zhai, A., Liu, B., Fang, B., Cai, C., Ma, E., Yin, E., Wang, H., Zhou, H., Wang, J., Shi, L., Liang, L., Wang, M., Wang, Q., Gan, R., Yu, R., Li, S., Liu, S., Chen, S., Chen, V., Xu, Z.: Igniting vlms toward the embodied space. arXiv preprint arXiv:2509.11766 (2025)
40. Zhang, D., Li, Z., Zhang, M., Zhang, J., Liu, Z., Yao, Y., Xu, H., Zheng, J., Wang, P., Chen, X., et al.: From system 1 to system 2: A survey of reasoning large language models. IEEE Transactions on Pattern Analysis and Machine Intelligence (2025)

41. Zhang, K., Xu, R., Ren, P., Lin, J., Wu, H., Lin, L., Liang, X.: Robridge: A hierarchical architecture bridging cognition and execution for general robotic manipulation. In: Proceedings of the IEEE/CVF International Conference on Computer Vision (ICCV). pp. 14590–14601. IEEE (2025)
42. Zhang, R., Isola, P., Efros, A.A., Shechtman, E., Wang, O.: The unreasonable effectiveness of deep features as a perceptual metric. In: Proceedings of the IEEE Conference on Computer Vision and Pattern Recognition (CVPR). pp. 586–595. IEEE (2018)
43. Zhang, R., Sun, Y., Zhang, Z., Li, J., Liu, X., Au, H.F., Guo, H., Yan, P.: Marl-mambacontour: Unleashing multi-agent deep reinforcement learning for active contour optimization in medical image segmentation. In: Proceedings of the 33rd ACM International Conference on Multimedia (MM). pp. 7815–7824. ACM (2025)
44. Zhang, R., Tian, K., Zhang, Z., Liu, Q., Jin, Z.: Fdg-diff: Frequency-domain-guided diffusion framework for compressed hazy image restoration. arXiv preprint arXiv:2501.12832 (2025)
45. Zhang, R., Yan, P., Zhang, Z., Chang, Y., Chen, H., Jin, Z.: Rpd-diff: Region-adaptive physics-guided diffusion model for visibility enhancement under dense and non-uniform haze. arXiv preprint arXiv:2508.16956 (2025)
46. Zhang, R., Zhou, J., Xu, Z., Liu, Z., Huang, J., Zhang, M., Sun, Y., Li, X.: Zero-shot 3d-aware trajectory-guided image-to-video generation via test-time training. arXiv preprint arXiv:2509.06723 (2025)
47. Zhang, Y., Zhong, Z., Liu, M., Chen, Z., Wu, B., Zeng, Y., Zhan, C., He, Y., Huang, J., Zhou, W.: Musetalk: Real-time high-fidelity video dubbing via spatio-temporal sampling. arXiv preprint arXiv:2410.10122 (2025)
48. Zhang, Z., Liao, J., Li, M., Dai, Z., Qiu, B., Zhu, S., Qin, L., Wang, W.: Tora: Trajectory-oriented diffusion transformer for video generation. In: Proceedings of the IEEE/CVF Conference on Computer Vision and Pattern Recognition (CVPR). pp. 2063–2073. IEEE (2025)
49. Zhang, Z., Chang, S., He, Y., Han, Y., Tang, J., Wang, F., Zhuang, B.: Blockvid: Block diffusion for high-quality and consistent minute-long video generation. arXiv preprint arXiv:2511.22973 (2025)
50. Zheng, D., Huang, Z., Liu, H., Zou, K., He, Y., Zhang, F., Zhang, Y., He, J., Zheng, W.S., Qiao, Y., Liu, Z.: Vbench-2.0: Advancing video generation benchmark suite for intrinsic faithfulness. arXiv preprint arXiv:2503.21755 (2025)
51. Zhong, Z., Ji, Y., Kong, Z., Liu, Y., Wang, J., Feng, J., Liu, L., Wang, X., Li, Y., She, Y., Qin, Y., Li, H., Mao, S., Liu, W., Luo, W.: Anytalker: Scaling multi-person talking video generation with interactivity refinement. arXiv preprint arXiv:2511.23475 (2025)
52. Zhou, J., Li, J., Xu, Z., Li, H., Cheng, Y., Hong, F.T., Lin, Q., Lu, Q., Liang, X.: Fireedit: Fine-grained instruction-based image editing via region-aware vision language model. In: Proceedings of the IEEE/CVF Conference on Computer Vision and Pattern Recognition (CVPR). pp. 13093–13103. IEEE (2025)
53. Zhou, S., Du, Y., Chen, J., Li, Y., Yeung, D.Y., Gan, C.: Robodreamer: Learning compositional world models for robot imagination. arXiv preprint arXiv:2404.12377 (2024)
54. Zhu, F., Wu, H., Guo, S., Liu, Y., Cheang, C., Kong, T.: Irasim: A fine-grained world model for robot manipulation. In: Proceedings of the IEEE/CVF International Conference on Computer Vision (ICCV). pp. 9834–9844. IEEE (2025)
55. Zhu, F., Yan, Z., Hong, Z., Shou, Q., Ma, X., Guo, S.: Wmpo: World model-based policy optimization for vision-language-action models. arXiv preprint arXiv:2511.09515 (2025)

# Supplementary Material

## 6 Analysis of Computational Cost and Hyperparameters

This section provides a detailed analysis of the computational cost and key hyperparameters of the MIND-V framework. We first examine the world model’s scalability with respect to task length and then present an ablation study on the number of staged visual future rollouts ( $K$ ) utilized in our test-time optimization strategy.

### 6.1 Scalability with Task Length

To validate MIND-V’s efficiency as a world simulator in long-horizon tasks, we measure the simulation time and peak VRAM usage across tasks ranging from one to three sub-tasks. The key metrics are summarized in Table 6 and visualized in Figure 7.

Our findings highlight two critical properties of the proposed architecture. First, the total simulation time scales linearly with the number of sub-tasks. The average time per sub-task remains constant at approximately 60 seconds<sup>1</sup>, demonstrating that our framework’s computational time scales predictably with task length. Second, and crucially, the peak VRAM usage remains constant regardless of the task length. As shown by the consistently sized circles in Figure 7, the peak VRAM remains constant at approximately 70 GB. This constant memory footprint is a direct benefit of our hierarchical and autoregressive design, where memory is allocated for a single sub-task and subsequently reused, enabling highly scalable visual world simulation for long task sequences.

**Table 6: Computational cost as a function of task length.** We report total time, average time per sub-task, peak VRAM usage, and the percentage distribution of time and VRAM across the SRH planning and MVG simulation stages.

No. of Sub-tasks	Total Time (s)	Avg. Time per Peak VRAM		Time Dist. (%)		VRAM Dist. (%)	
		Sub-task (s)	(GB)	Plan (SRH)	Gen (MVG)	Plan (SRH)	Gen (MVG)
1	60.24	30.14	70.12	36.5%	63.5%	14.1%	85.9%
2	123.02	30.60	70.12	34.3%	65.7%	14.4%	85.6%
3	181.55	30.85	70.12	32.4%	67.6%	14.0%	86.0%

Furthermore, Table 6 details the internal resource distribution. The Motor Video Generator (MVG) constitutes the primary computational bottleneck, consuming the majority of both execution time (approximately 65-70%) and VRAM

<sup>1</sup>This is a reference value using the Gemini-2.5 API [8]. The inference speed of the SRH is influenced by multiple factors, including VLM API response time and network latency. Reported times represent pure inference duration, excluding network transmission latency.

(approximately 86%). In contrast, the Semantic Reasoning Hub (SRH) planning stage introduces only a minor and stable computational overhead.

## 6.2 Analysis of the Number of Rollout Samples ( $K$ )

The Staged Visual Future Rollouts mechanism is governed by a key hyperparameter,  $K$ , which defines the number of candidate future trajectories simulated at each sub-task transition. While a larger  $K$  increases the probability of identifying a physically plausible future, it also incurs greater computational cost. To analyze this trade-off, we conduct an ablation study by varying  $K$  from 1 to 5.

The results, visualized in Figure 8, illustrate the relationship between simulation fidelity and computational cost. As shown in the performance radar chart (Figure 8, left), a significant performance uplift is observed as  $K$  increases from 1 to 3, demonstrating the effectiveness of the rollout mechanism in filtering out physically incoherent futures. For instance, the Task Success Rate increases from 35.2% at  $K=1$  to 61.3% at  $K=3$ . However, this trend exhibits sharply diminishing returns, with only marginal gains when increasing  $K$  from 3 to 5. In contrast, the computational cost scales unfavorably with larger  $K$  as shown in the bar chart (Figure 8, right). For example, Peak VRAM consumption nearly doubles from 70.1 GB at  $K=3$  to 122.0 GB at  $K=5$ . This analysis confirms that  $K=3$  strikes an optimal balance between simulation accuracy and computational efficiency. Therefore, we adopt  $K=3$  as the default setting for all experiments.

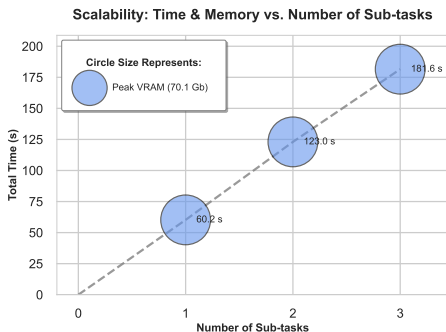


**Fig. 7: Scalability of MIND-V.** Total generation time (Y-axis) scales linearly with the number of sub-tasks (X-axis). Circle size represents peak VRAM, which remains constant, demonstrating the memory efficiency of our approach.

## 7 Dataset Construction

The Supervised Fine-Tuning (SFT) stage of our training paradigm requires a large-scale dataset of robotic manipulation videos annotated with our structured Behavioral Semantic Bridge (BSB) representation. To this end, we developed an automated pipeline to generate ground-truth BSB annotations from the raw Bridge V2 dataset [31] following the data processing protocol established in [10], as illustrated in Figure 9. This pipeline comprises two primary stages: Object Representation Generation and Trajectory Decomposition.

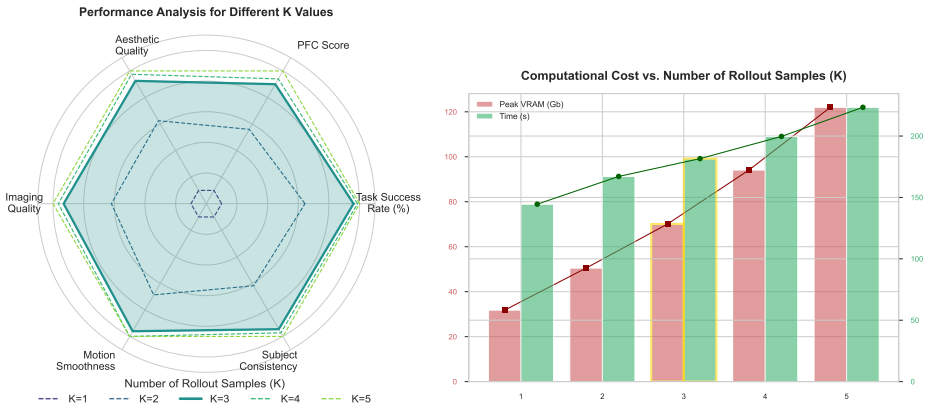


**Fig. 8: Analysis of the trade-off for the number of visual future rollouts ( $K$ ).** (Left) The performance radar chart shows that the overall performance area expands significantly up to  $K=3$  but exhibits diminishing returns thereafter. (Right) The cost chart shows that both time and Peak VRAM increase steadily with  $K$ , with memory cost escalating significantly.  $K=3$  (highlighted) is chosen as the optimal balance.

**Table 7: Ablation study on the number of visual future rollouts ( $K$ ).** We evaluate the impact of varying  $K$  on functional correctness, visual quality, and computational cost. The setting  $K=3$  (highlighted row) achieves the best balance between performance and efficiency.

$K$	Cost		Performance					
	Time (s) ↓	Peak VRAM (GB) ↓	Task Success Rate (%) ↑	PFC Score ↑	Aesthetic Quality ↑	Imaging Quality ↑	Motion Smoothness ↑	Subject Consistency ↑
1	144.5	31.8	35.2	0.405	0.471	0.660	0.931	0.865
2	167.1	50.5	51.7	0.428	0.492	0.675	0.946	0.884
<b>3</b>	<b>181.6</b>	<b>70.1</b>	<b>61.3</b>	<b>0.445</b>	<b>0.504</b>	<b>0.684</b>	<b>0.953</b>	<b>0.896</b>
4	199.7	94.1	62.1	0.447	0.506	0.685	0.954	0.897
5	223.4	122.0	62.5	0.450	0.507	0.686	0.954	0.898

## 7.1 Object Representation Generation

This stage derives the **Object Representation** (segmentation masks) for both the manipulated object ( $M_{\text{obj}}$ ) and the robot arm ( $M_{\text{rob}}$ ) by visually grounding the natural language instructions. For each sub-task video and its corresponding instruction (e.g., “pick up the red block”), the extraction process proceeds as follows:

- Object Identification:** A pre-trained Vision-Language Model (VLM), such as Qwen-VL 2.5 [3], extracts the noun phrase corresponding to the object of manipulation (e.g., “red block”) from the instruction.
- Language-Grounded Segmentation:** The extracted noun phrase serves as a text prompt for Grounded SAM2 [29], an open-vocabulary segmenta-

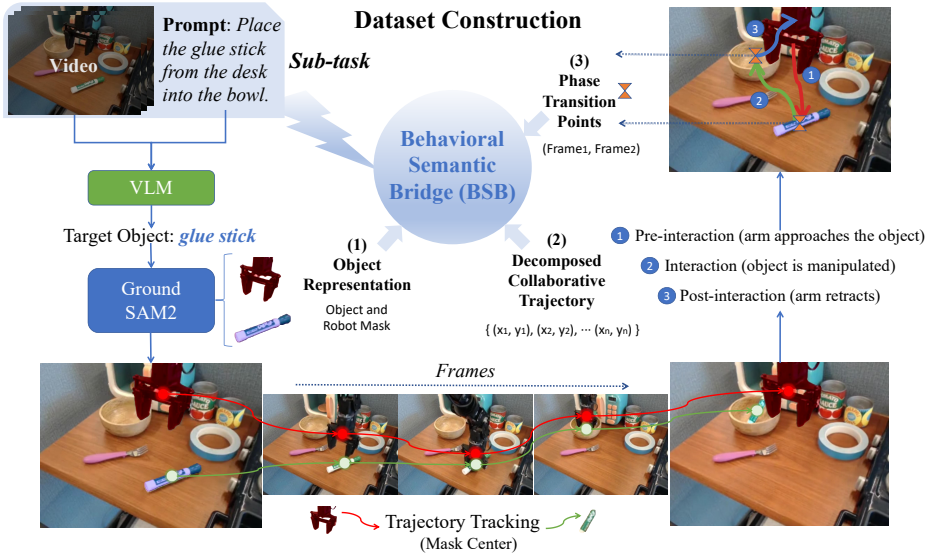


**Fig. 9: Overview of our automated BSB annotation pipeline.** A VLM first extracts the target object from the language prompt, which is then used by Grounded SAM2 [29] to generate the (1) Object Representation (masks). Concurrently, trajectory tracking is performed on the object and gripper masks. The trajectory is partitioned based on the object’s motion to produce the (2) Decomposed Collaborative Trajectory and (3) Phase Transition Points. These components collectively form the structured BSB annotation used for SFT.

tion model, which generates the pixel-wise segmentation mask for the target object ( $M_{obj}$ ) in the initial frame.

3. **Robot Arm Mask:** Because the manipulator’s visual appearance remains consistent across the dataset, we apply a pre-defined template mask to obtain the robot arm segmentation ( $M_{rob}$ ).

## 7.2 Trajectory Decomposition and Phase Segmentation

This stage tracks and partitions the trajectories of the robot and the object into three meaningful phases: pre-interaction, interaction, and post-interaction. The process is based on the motion state of the manipulated object.

We first employ a video object tracking model, in this case SAM2 [28], to track the segmentation masks of both the target object and the robot gripper throughout the video sequence. The center point of these masks forms the raw trajectory data. The **Decomposed Collaborative Trajectory** is then segmented based on the object’s motion:

1. **Pre-interaction Phase ( $T_{pre}$ ):** This phase is defined as the sequence of frames from the start of the sub-task until the target object begins to move.

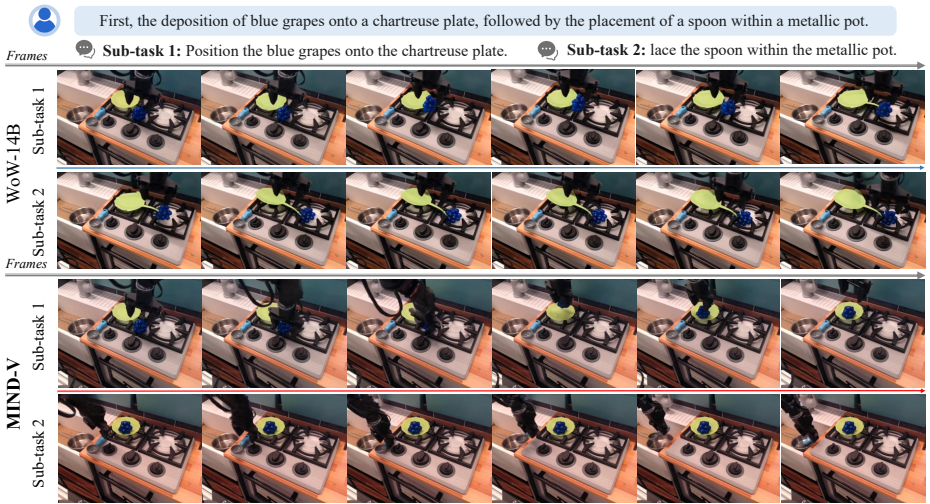


**Fig. 10: Qualitative comparison on a complex long-horizon task.** The model is instructed to first place blue grapes onto a chartreuse plate, and then place a spoon into a metallic pot. **(Top)** The baseline model, WoW-14B [7], exhibits a catastrophic failure in long-horizon reasoning. In Sub-task 1, the grapes levitate without being touched, a clear physical violation. In Sub-task 2, it demonstrates severe semantic grounding error by incorrectly interacting with the plate instead of the instructed spoon, resulting in a complete breakdown of logical coherence. **(Bottom)** In stark contrast, MIND-V successfully executes the full sequence, correctly completing both sub-tasks as instructed. This result validates the efficacy of our hierarchical architecture; the SRH’s explicit planning and the BSB’s structured guidance prevent the semantic drift and error accumulation that plague the baseline, ensuring robust execution of multi-step instructions.

2. **Interaction Phase** ( $T_{interact}$ ): This phase covers the frames during which the target object is in motion.
3. **Post-interaction Phase** ( $T_{post}$ ): This phase begins once the target object comes to rest again and continues until the end of the sub-task.

The spatiotemporal trajectories of the robot arm and the manipulated object are determined by the paths of their respective mask centroids during these phases. The **Phase Transition Points** ( $F_{pre}, F_{interact}, F_{post}$ ) are defined by the start and end points of the object’s motion. To ensure fidelity of world dynamics, failure cases from the automated pipeline, such as incorrect grounding or trajectory errors, are flagged for manual correction by human annotators.

## 8 Additional Visual Results

This section presents a comprehensive qualitative evaluation comparing MIND-V against state-of-the-art baselines. We analyze performance across three distinct regimes, including multi-stage long-horizon manipulation tasks shown in

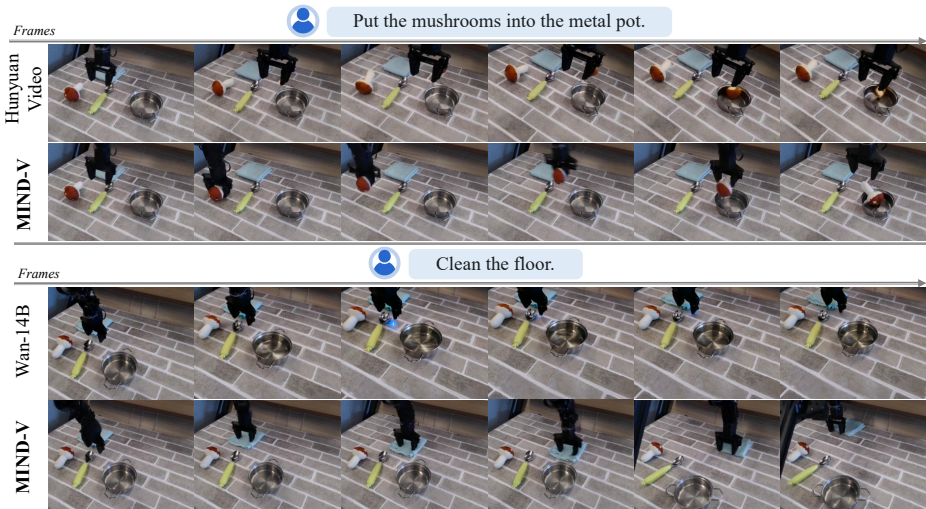


**Fig. 11: Qualitative comparison on short-horizon tasks.** This figure illustrates performance on two distinct single-step instructions. **(Top)** For “Put the mushrooms into the metal pot”, the baseline (HunyuanVideo [19]) exhibits physical implausibility, with the mushroom clipping through the pot’s rim. MIND-V, in contrast, simulates a physically plausible interaction. **(Bottom)** For the more abstract instruction “Clean the floor”, the baseline (Wan-14B [32]) fails to take any action, demonstrating a lack of semantic grounding. MIND-V correctly interprets the instruction, grasps the cloth, and performs a wiping motion, showcasing its superior planning and reasoning capabilities.

Figure 10, atomic short-horizon interactions illustrated in Figure 11, and generalization to complex out-of-distribution (OOD) scenarios with diverse action primitives as depicted in Figure 12. These visualizations substantiate our quantitative findings, showcasing MIND-V’s superiority as a physically grounded and logically coherent world simulator.

**Long-horizon Tasks.** As illustrated in Figure 10, baseline models exhibit a clear breakdown in long-horizon tasks. They not only violate physical common sense within a individual sub-task but also fail to maintain causal consistency across the temporal sequence. For instance, baseline attempts to interact with an object that spontaneously disappeared in a previous step highlight a profound failure in tracking latent world states. In contrast, MIND-V maintains robust logical coherence throughout the sequence. This success stems from our hierarchical design: the Semantic Reasoning Hub (SRH) explicitly decomposes complex instructions into structured sub-tasks, while the Staged Visual Future Rollouts mechanism actively filters physically implausible transitions, effectively preventing long-term semantic drift.

**Short-horizon Tasks.** The short-horizon examples in Fig. 11 further emphasize the physical fidelity of our approach. Even when baselines correctly identify target objects, they frequently hallucinate physically impossible interactions,

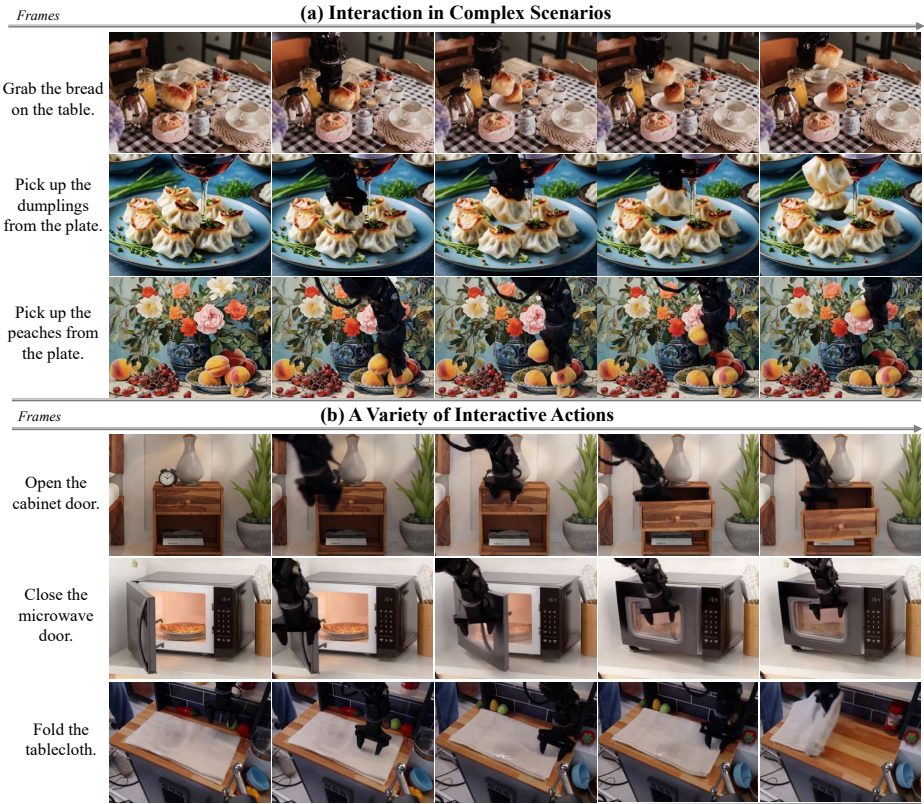


**Fig. 12: Generalization to complex scenarios and diverse manipulation skills.** Panel (a) demonstrates the robust generalization ability of MIND-V in out-of-distribution (OOD) scenarios. The world model accurately isolates and manipulates targets in cluttered environments (e.g., grabbing bread from a full table or picking a dumpling), as well as in stylistically distinct scenes (e.g., picking peaches in an artistic setting). The domain-invariant BSB representation ensures precise control without disturbing the background fidelity. Panel (b) highlights the simulation of diverse interactive dynamics where the model leverages affordance-aware reasoning to execute physics-compliant interactions. This includes manipulating articulated objects like opening a cabinet or closing a microwave, as well as handling deformable materials such as folding a tablecloth.

such as objects levitating without contact or penetrating solid surfaces. Our GRPO-based physical alignment successfully mitigates these dynamic violations. Furthermore, MIND-V excels at interpreting abstract commands (e.g., “clean the floor”) by autonomously inferring the correct latent action sequence (grasping a cloth, then wiping). This demonstrates the SRH’s cognitive capacity to translate high-level intent into executable, physically grounded trajectories—a key differentiator from monolithic models that struggle with action grounding.

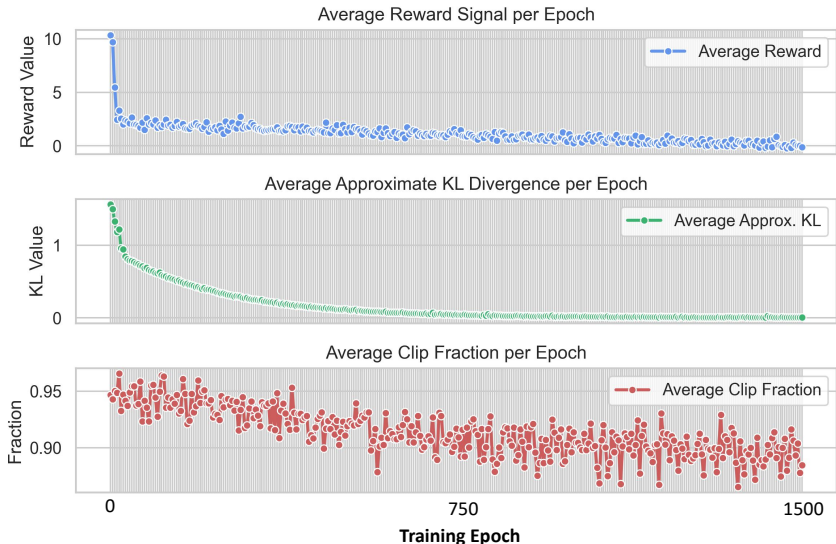


**Fig. 13: GRPO post-training epoch-level dynamics.** Visualization of key metrics, averaged at the end of each epoch. The reward signal shows a clear upward trend, while the KL divergence and clip fraction both exhibit stable convergence, indicating an effective and well-behaved optimization process.

**Complex OOD Scenarios and Diverse Interactive Actions.** Fig. 12 demonstrates the robust generalization capabilities that are the hallmark of a scalable world model. Panel (a) illustrates the model’s precision in visually diverse OOD environments. Whether distinguishing a specific object within severe clutter or operating in a stylized scene, MIND-V accurately executes the intent. Crucially, the background remains strictly static despite high-frequency textures. This stability is achieved because the Behavioral Semantic Bridge (BSB) decouples semantic intent from visual appearance, providing structural, domain-invariant guidance to the diffusion process. Panel (b) highlights MIND-V’s ability to model complex physical state transitions. The model effortlessly simulates interactions with articulated objects (e.g., cabinets) and deformable materials (e.g., cloth). Executing these actions requires deep kinematic and affordance understanding, proving that integrating the SRH’s cognitive reasoning with the MVG’s simulation engine creates a highly capable embodied world model.

## 9 Analysis of GRPO Post-Training

To provide insight into the stability and effectiveness of our GRPO post-training phase, we visualize key training metrics on an epoch-by-epoch basis in Figure 13. For clarity, the plots show the average value of each metric at the end of each epoch. The curves illustrate clear, convergent trends for the policy loss (reward signal), approximate KL divergence, and clip fraction.

The training curves demonstrate a stable and effective optimization process:

**Table 8: Detailed architecture and data flow of the Motor Video Generator (MVG).** The table shows the transformation of tensor shapes from the input video and BSB guidance through each major component. Notations: B=Batch Size, C=Channels, T=Temporal Length, H=Height, W=Width, L=Sequence Length, D=Embedding Dimension.

Component	Module	Input Shape	Output Shape	Key Hyperparameters
3D VAE	Encoder	[B, 3, T, H, W]	[B, 16, T/4, H/8, W/8]	Latent Channels: 16
	Decoder	[B, 16, T/4, H/8, W/8]	[B, 3, T, H, W]	Symmetrical to Encoder
Guidance Embedding	Guidance Tensor	BSB	[B, 128, T/4, H/8, W/8]	Encodes BSB masks & trajectories into a dense tensor.
	Spatial Conv	[B, 128, T/4, H/8, W/8]	[B, 480, T/4, H/8, W/8]	Kernel: 3x3, Stride: 1
	Temporal Conv	[B, 480, T/4, H/8, W/8]	[B, 1920, T/4, H/8, W/8]	Kernel: 3 (1D), Stride: 1
DiT Backbone (30 Blocks)	Patch Embedding	[B, 16, T/4, H/8, W/8]	[L, D]	Patch Size: 2x2x2, Hidden Dim (D): 1920
	Positional Encoding	[L, D]	[L, D]	Type: 3D Sinusoidal
	Timestep Embedding	Scalar $t$	[1, 512]	-
	Transformer Blocks	[L, D]	[L, D]	Layers: 30, Attention Heads: 30, Head Dim: 64
	Scheduler	DDIM	Scalar $t$	Noise Schedule

- **Convergent Reward Optimization:** The average reward signal per epoch exhibits a clear and steady upward trend. This indicates that the policy is successfully and progressively optimizing for the desired objectives of physical plausibility and aesthetic quality.
- **Stable Policy Updates:** The average approximate KL divergence shows a clear downward trend, gradually converging towards a low, stable value. This signifies that the policy updates become smaller and more refined as training progresses, demonstrating stable convergence without drastic policy shifts.
- **Well-Calibrated Optimization:** The average clip fraction also steadily decreases, indicating that as the policy improves, fewer updates are being clipped. This confirms that the optimization is proceeding smoothly and that the learning rate and clipping hyperparameters are well-calibrated.

Collectively, these convergent trends validate that our GRPO post-training is a stable and effective process. It progressively steers the generator towards higher physical fidelity and aesthetic quality, successfully aligning the model with abstract, hard-to-define objectives.

## 10 Network Architecture Details

This section details the architectural design and data flow of the Motor Video Generator (MVG). Built upon the CogVideoX-5B [37] foundation, the MVG employs a 3D Variational Autoencoder (VAE) and a Diffusion Transformer (DiT) [27] backbone. Our primary modification is the conditioning mechanism,

which injects explicit spatiotemporal guidance from the Behavioral Semantic Bridge (BSB) to achieve precise kinematic control. The key module specifications and tensor transformations are summarized in Table 8 and elaborated below.

**Latent Space Definition.** The MVG operates within a compressed latent space parameterized by a pre-trained 3D-VAE [17]. As detailed in Table 8, the VAE encoder performs spatiotemporal compression on an input video of shape  $[B, 3, T, H, W]$ , producing a compact latent representation of shape  $[B, 16, T/4, H/8, W/8]$ . The entire forward and reverse diffusion processes are executed within this latent space. Subsequently, the VAE decoder maps the final denoised latent back to the pixel space to render the simulated video.

**Diffusion Transformer Backbone.** The core of the MVG simulation engine is a 30-block DiT with a hidden dimension of 1920. The latent video is first partitioned into non-overlapping  $2 \times 2 \times 2$  spatiotemporal patches, which are linearly embedded into a sequence of tokens. This token sequence is augmented with 3D sinusoidal positional encoding and diffusion timestep embeddings prior to being processed by the transformer blocks.

**BSB Conditioning Mechanism.** To enforce action adherence, the conditioning mechanism integrates BSB guidance directly into the DiT backbone via a **Guidance Embedding** module. Initially, the structured semantic information from the BSB is rasterized into a dense Spatiotemporal Guidance Tensor. This tensor is processed by a sequence of spatiotemporal convolutions—specifically, a  $3 \times 3$  spatial convolution followed by a 1D temporal convolution—yielding a 1920-dimensional feature representation,  $G$ . This guidance signal, maintaining identical spatiotemporal resolution to the latent video, is injected into the DiT backbone via additive fusion. This injection is performed exclusively within the even-numbered transformer blocks (e.g., blocks 0, 2, 4, ...), leaving the odd-numbered blocks unconditioned. This alternating fusion strategy effectively interleaves explicit kinematic control from the BSB with the model’s internal video generation priors, steering the denoising trajectory to strictly adhere to the planned trajectory.